



HAL
open science

Lithium electrochemical deintercalation from O₂-LiCoO₂: structure and physical properties

Dany Carlier-Larregaray, Ismaël Saadoune, Michel Ménétrier, Claude Delmas

► **To cite this version:**

Dany Carlier-Larregaray, Ismaël Saadoune, Michel Ménétrier, Claude Delmas. Lithium electrochemical deintercalation from O₂-LiCoO₂: structure and physical properties. Journal of The Electrochemical Society, 2002, 149 (10), pp.A1310-A1320. 10.1149/1.1503075 . hal-00817889

HAL Id: hal-00817889

<https://hal.science/hal-00817889>

Submitted on 3 Jan 2024

HAL is a multi-disciplinary open access archive for the deposit and dissemination of scientific research documents, whether they are published or not. The documents may come from teaching and research institutions in France or abroad, or from public or private research centers.

L'archive ouverte pluridisciplinaire **HAL**, est destinée au dépôt et à la diffusion de documents scientifiques de niveau recherche, publiés ou non, émanant des établissements d'enseignement et de recherche français ou étrangers, des laboratoires publics ou privés.

Lithium Electrochemical Deintercalation from O2-LiCoO₂

Structure and Physical Properties

D. Carlier,^a I. Saadouné,^{a,b} M. Ménétrier,^a and C. Delmas^{a,*}

^aInstitut de Chimie de la Matière Condensée de Bordeaux-CNRS and Ecole Nationale Supérieure de Chimie et Physique de Bordeaux, Université de Bordeaux I, 33608 Pessac cedex, France

^bDépartement de Chimie, Faculté des Sciences et Techniques, 40 000 Marrakech, Morocco

Electrochemical deintercalation of Li from the metastable O2-LiCoO₂ phase has been investigated up to the composition Li_{0.15}CoO₂. The single-phase domains that separate the voltage plateaus observed have been characterized by X-ray diffraction. The succession of phases observed upon deintercalation results from reversible sheet gliding or lithium/vacancy ordering, leading to the sequence O2, T[#]2, T[#]2', O6, O2, O2. In particular, the T[#]2 stacking, similar to the T2 phase reported by Dahn and co-workers for the Li_{2/3}Ni_{1/3}Mn_{2/3}O₂ phase, corresponds to oxygen ions not sitting on the three positions of a triangular lattice, hence the # character is used. It exhibits very distorted tetrahedral sites for Li. The O6 stacking exhibits two kinds of CoO₆ octahedra, which might allow Co³⁺/Co⁴⁺ ordering in alternate sheets. The most deintercalated O2-Li_{0.15}CoO₂ phase has never been reported before. Electronic properties and ⁷Li magic-angle spinning nuclear magnetic resonance show a transition to a metallic state for $x < 0.94$ (appearance of the T[#]2 phase with $x = 0.72$). These stacking changes are proposed to result from the minimization of electrostatic repulsion, except for T[#]2' ($x = 0.50$), which is believed to result from a Li/vacancy ordering.

LiCoO₂ can exhibit two types of layered structures depending on its preparation method. The thermodynamically stable variety is prepared by a solid-state reaction and exhibits an O3 stacking where the LiO₆ and CoO₆ octahedra share only edges. The O2-type LiCoO₂ is metastable and was prepared for the first time by Delmas *et al.* by an Na⁺/Li⁺ exchange from the P2-Na_{0.70}CoO₂ phase.¹ In this structure, the LiO₆ octahedra share edges but also faces with the CoO₆ ones as shown in Fig. 1. Two CoO₂ layers are needed to describe the unit cell so that this new packing was called O2, in agreement with the packing designation proposed previously for the layered AMO₂ phases (A = alkaline, M = transition metal).² The P, T, or O letter describes the alkali ion site (prismatic, tetrahedral, or octahedral, respectively) and the number 1, 2, or 3 indicates the number of slabs within the hexagonal cell.

Recently, we undertook a new investigation of the O2-LiCoO₂ system from the structural and physical properties point of view.³ The magnetic properties and a ⁷Li nuclear magnetic resonance (NMR) study show that the O2 starting phase exhibits a composition very close to the ideal one with low spin Co³⁺ ions. Rietveld refinement of the structure in the hexagonal *P6₃mc* space group from the neutron diffraction pattern indicates that the repulsion between lithium and cobalt ions through the common face of their octahedra is strong enough to displace them from the center of their octahedra.

To our knowledge, very few papers deal with the O2-LiCoO₂ used as positive electrodes in lithium-ion batteries. The first study was reported by Mendiboure *et al.*,⁴ who characterized by X-ray diffraction (XRD) the deintercalated Li_{*x*}CoO₂ phases. Very recently, Dahn and co-workers were interested in the O2 stacking. They studied the electrochemically deintercalated O2-Li_{*x*}CoO₂ phases by *in situ* XRD and confirmed to a large extent the results previously reported by Mendiboure *et al.*⁵ They, however, noticed that in the $0.5 < x < 0.7$ composition range, the XRD patterns give evidence of a new oxygen packing that they characterized in the case of Li_{2/3}Ni_{1/3}Mn_{2/3}O₂.⁶ They also showed evidence for the reformation of the O2 stacking for highly deintercalated phases. They showed that the electrochemical properties of the O2-LiCoO₂ are competitive with those of the conventional O3-LiCoO₂ and their differential

scanning calorimetry (DSC) measurements indicate that the O2-Li_{*x*}CoO₂ system charged up to 4.2 V is about as safe as the O3 one at the same potential.⁵

We report in the present paper a detailed study of the structural and physical properties of the Li_{*x*}CoO₂ phases obtained by electrochemical deintercalation from the O2-type LiCoO₂.

Experimental

Preparation of O2-LiCoO₂.—O2-LiCoO₂ was prepared by ion exchange reaction from P2-Na_{0.70}CoO₂. The Na_{0.70}CoO₂ precursor material was prepared by the solid-state reaction of a mixture of Na₂O (Aldrich, 5% excess) and Co₃O₄ [obtained from Co(NO₃)₂·6H₂O Carlo Erba 99% min at 450°C for 12 h under O₂] at 800°C under O₂ for 48 h. The mixture was ground and pelletized in a dry box (under argon) before the heat-treatment, and was then quenched into liquid N₂ in order to fix the oxygen stoichiometry. Ion-exchanging sodium for lithium in the P2 phase can be performed in an aqueous solution of lithium ions.^{3,7} An LiCl/LiOH (1:1) solution in water (5 M) was used and the exchange was performed during 24 h with an intermediate washing, drying, and grinding. An excess of lithium was used (Li/Na = 10) and the exchanged phase was washed and dried under vacuum at 100°C for around 14 h.

Electrochemical studies.—Electrochemical studies were carried out with Li/liquid electrolyte/O2-LiCoO₂ cells. LiPF₆ in ethylene carbonate-dimethyl carbonate-propylene carbonate (Merck, ZV1011 Selectipur) was used as electrolyte. The cells were assembled in an argon-filled dry box.

For classical electrochemical experiments, the positive electrode consisted of a mixture of 86% by weight of active material, 4% of polytetrafluoroethylene (PTFE) and 10% of carbon black and a C/40 current density was used (*i.e.*, 40 h are needed to remove 1 mol of lithium).

For preparation of the phases used for the XRD Rietveld acquisition, a large cell was used (≈ 700 mg of active material). The starting O2-LiCoO₂ phase was mixed with 10% by weight of carbon black, but no binder was used. These cells were charged at low current density (C/100).

For the electrochemical preparation of deintercalated phases for ⁷Li magic-angle spinning (MAS) NMR and electrical measurements, pellets (4 tons for an 8 mm diam) of the starting material were used as the positive electrode without an additive. However, because of

* Electrochemical Society Active Member.

^z E-mail: delmas@icmcb.u-bordeaux.fr

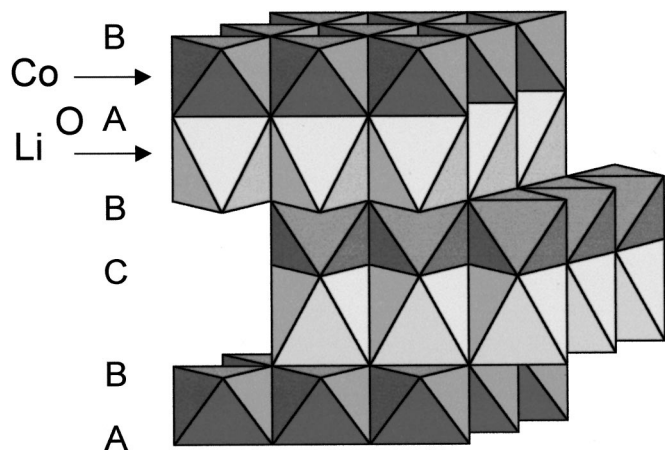


Figure 1. The O2 stacking of LiCoO₂.

the metastability of the O2-LiCoO₂ phase, no thermal treatment of the pellets could be done to improve the internal contacts in the material. These cells were charged at very low current density ($C/600$).

X-ray diffraction (XRD).—The XRD patterns of the deintercalated phases were recorded using a Philips PW1050 powder diffractometer with Cu K α radiation and a graphite diffracted beam monochromator, from 10 to 80° or 110° (2θ) with a 0.02° step and a 10 s counting time by step.

The XRD patterns for the Rietveld analysis were collected at room temperature from 10 to 120° (2θ) with a 0.02° step and a 40 s counting time by step, using a Siemens D5000 powder diffractometer with the Cu K α radiation and a graphite diffracted beam monochromator. The samples were carefully prepared in order to avoid strong preferential orientation.

The structure refinements were performed from powder diffraction data using the Fullprof program with a pseudo-Voigt fitting function.⁸

NMR experiments.—⁷Li MAS NMR spectra were recorded on a Bruker MSL200 spectrometer at 77.7 MHz, with a standard Bruker MAS probe. The samples were mixed with dry silica (typically 50% in weight) and were placed into 4 mm diam zirconia rotors. Spinning frequencies (ν_r) of 10–13 kHz were used. Two types of sequences were used, a single pulse sequence and a rotor-synchronized echo pulse sequence [$t_{\pi/2} - \tau_1 - t_{\pi} - \tau_2$] with a 90° pulse duration ($t_{\pi/2}$) of 3.5 μ s.⁹ A 200 kHz spectral width was used and the recycle time $D_0 = 1$ s, was long enough to avoid T_1 saturation effects. The single-pulse sequence requires a first-order phasing process and a $\sin x/x$ baseline correction due to the dead time of the spectrometer. The isotropic shifts reported in parts per million are relative to an external sample of 1 M LiCl solution in water.

Electronic conductivity and thermoelectronic measurements.—For electronic conductivity measurements, a four-probe method was used with direct current in the 100–300 K range. The thermoelectronic measurements were carried out by using equipment described elsewhere.¹⁰

Results and Discussion

Electrochemical properties.—Figure 2 shows the cycling curve of an Li//O2-LiCoO₂ cell at the $C/40$ rate. Almost all the lithium can be reversibly extracted from the O2 phase when charged to 4.6 V. The corresponding capacity is high, 213 mAh/g for the first discharge between 4.6 and 3.5 V. As was shown by Mendiboure *et al.* and by Paulsen *et al.*, lithium deintercalation from O2-LiCoO₂ is associated with several reversible-phase transformations, that can

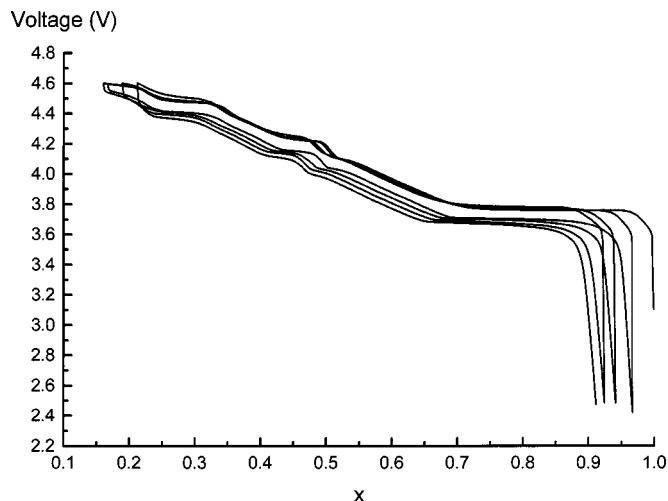


Figure 2. Cycling curve of a Li//O₂-LiCoO₂ cell obtained with a $C/40$ current density rate (40 h are needed to extract 1 mol of lithium).

result from reversible (CoO₂) sheets gliding, from lithium/vacancy ordering, or from a nonmetal to metal transition.^{4,5} Thus the layered structure remains at all points between $x = 1$ and $x = 0.16$ on the voltage curve.

No extra voltage plateau at 3.93 V, typical of the O3-Li_xCoO₂ system,¹¹ appears during cycling; this suggests that the O2 phase does not transform into the thermodynamically stable O3 one. Indeed, the O2 \rightarrow O3 transformation is not expected at room temperature since it involves breaking and reconstructing of the strong Co-O bonds. This observation is in good agreement with those reported by Paulsen *et al.*, they showed that several O2 systems do not convert to the more stable O3 stacking during cycling.^{5,12,13}

Recording the open-circuit voltage curve up to 4.30 V (Fig. 3) yields more precise values of the potential of the voltage plateaus up to this point. However, it does not provide accurate composition ranges for the single-phase domains as a small shift in x is observed as compared to Fig. 2. This could partly result from a decomposition of the electrolyte during the very long charge with relaxation periods experiment [the relaxation is interrupted when the slope of the $V = f(t)$ curve is smaller than 0.1 mV/h].

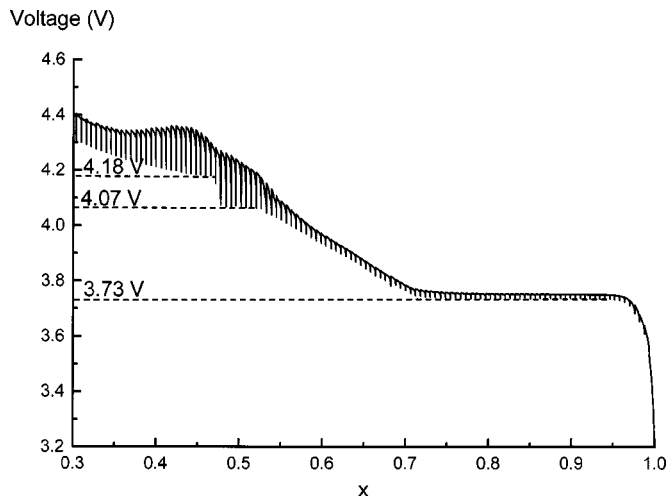


Figure 3. Open-circuit voltage curve of an Li//O₂-LiCoO₂ cell, obtained with a $C/100$ current density applied for 36 min steps and an end of relaxation criterion of $\Delta V/\Delta t = 0.1$ mV/h.

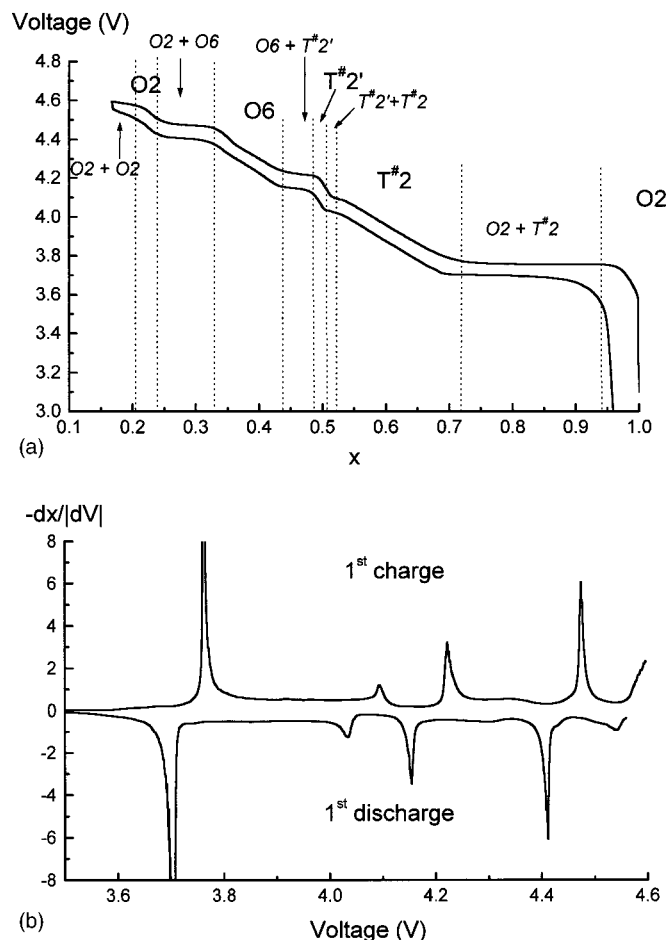


Figure 4. (a) First galvanostatic charge-discharge curve of a Li//O₂-LiCoO₂ cell obtained with a C/40 current density rate. (b) Differential $-dx/dV$ curve vs. voltage of the first galvanostatic charge-discharge curve.

Figure 4 shows the first galvanostatic charge and discharge curves of a Li//O₂-LiCoO₂ cell at the C/40 rate and the derivative $-dx/dV$ curve vs. voltage. The voltage plateaus are observed at the same potential as in Fig. 3. We first give here a general description of the charge/discharge curve; the XRD characterization of all the phases involved is described in the following paragraph.

$0.94 < x \leq 1$, O₂-Li_xCoO₂ single-phase domain. $0.72 < x \leq 0.94$: 3.73 V voltage plateau resulting from the existence of a two-phase domain and assigned to the O₂ → T[#]2 transformation. $0.52 < x \leq 0.72$: T[#]2-Li_xCoO₂ single-phase domain. $0.50 < x \leq 0.52$: 4.07 V voltage plateau resulting from the existence of a two-phase domain and assigned to the T[#]2 → T[#]2' transformation. $x \approx 0.50$: a narrow single-phase domain. The OCV curve clearly shows the presence of two plateaus at 4.07 and 4.18 V on both sides, which gives evidence for the existence of a single T[#]2' phase domain. This feature is quite similar to that observed for the O₃-Li_xCoO₂ system at the same x value. In the latter system, it was assigned to a lithium/vacancy ordering within the interslabs space, leading to a monoclinic cell distortion.¹¹ Paulsen *et al.* therefore suggested that one can also expect a lithium/vacancy ordering for $x = 0.50$ in the O₂ system.⁵ $0.42 < x < 0.50$: 4.18 V voltage plateau resulting from the existence of a two-phase domain and assigned to the T[#]2' → O₆ transformation. $0.33 < x < 0.42$: O₆-Li_xCoO₂ single-phase domain. $0.25 \leq x \leq 0.33$: 4.44 V voltage plateau resulting from the existence of a two-phase domain and assigned to the O₆ → O₂ transformation. $0.21 \leq x < 0.25$:

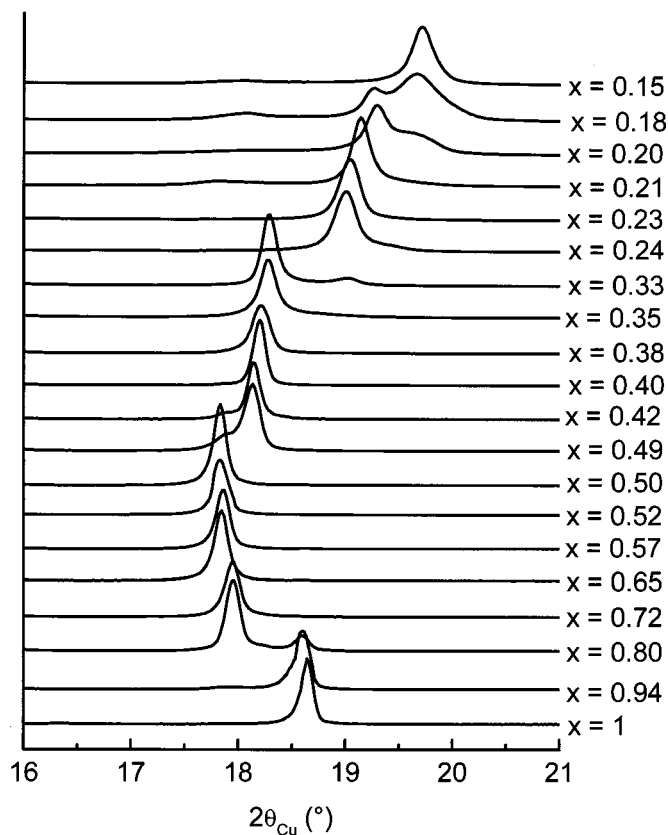


Figure 5. Evolution of the first XRD peak vs. lithium concentration in Li_xCoO₂ obtained by deintercalation of O₂-LiCoO₂.

O₂-Li_xCoO₂ single-phase domain. $0.18 \leq x < 0.21$: 4.57 V voltage plateau resulting from the existence of a two-phase domain and assigned to the O₂ → O₂ transformation. $x < 0.18$: highly deintercalated O₂-Li_xCoO₂ single-phase domain. As our cycling curve ends at 4.6 V, we do not observe the whole single-phase domain corresponding to this new O₂ phase on Fig. 4, so that we do not know the lower limit lithium concentration for its stability range.

Due to the stability limit of the electrolyte used, we could not cycle an O₂-LiCoO₂//Li battery in the whole lithium composition range.

XRD study.—In order to follow the changes in the crystal structure of O₂-LiCoO₂ during electrochemical deintercalation, XRD patterns of the Li_xCoO₂ samples were recorded. First, we verified by XRD that lithium reintercalation after a charge up to 4.6 V leads to an O₂ phase without any trace of the O₃ one, confirming the voltage profile analysis.

All the Li_xCoO₂ phases exhibit XRD patterns characteristic of layered materials. In this kind of compound, the interslab space is very sensitive to the amount of lithium and to the packing type and its evolution vs. the lithium amount can be followed by looking at the first diffraction peak. We therefore plotted the first diffraction line of some Li_xCoO₂ samples on Fig. 5. Figure 6 shows the complete XRD patterns of materials selected as characteristic of each type of phase, with the corresponding reflection assignment in the hexagonal system. Table I summarizes the cell parameters refined for each phase and Fig. 7 shows the evolution of the interslab space as a function of the lithium content.

O₂-Li_xCoO₂ ($0.94 < x \leq 1$).—The $0.94 < x \leq 1$ domain appears to be a solid solution with an O₂ stacking. In this narrow domain, the change in cell parameters is almost negligible.

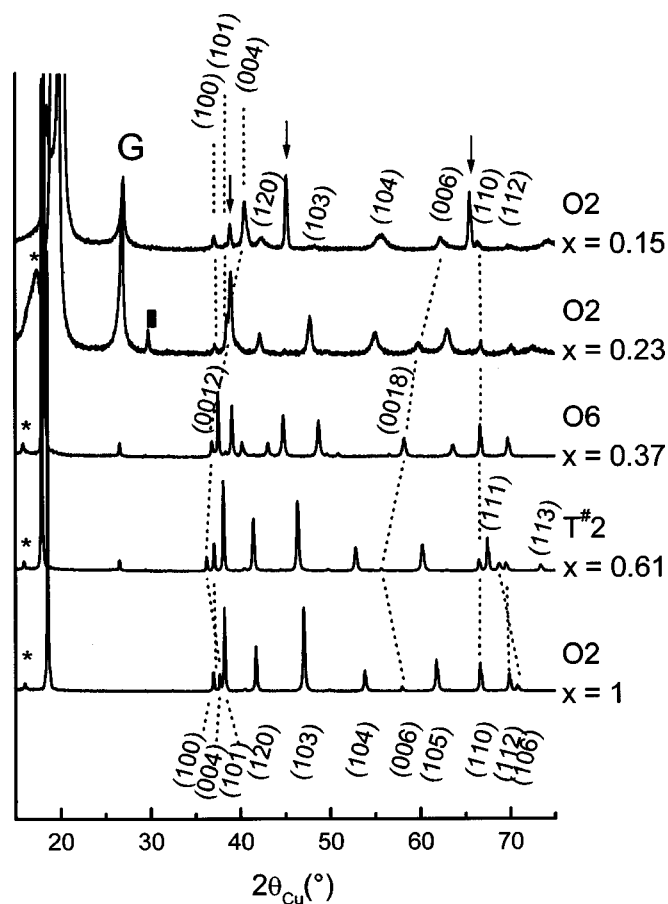


Figure 6. XRD patterns representing each type of phase observed for the Li_xCoO_2 system: the O2- LiCoO_2 starting phase, T[#]2- $\text{Li}_{0.61}\text{CoO}_2$, O6- $\text{Li}_{0.37}\text{CoO}_2$, O2- $\text{Li}_{0.23}\text{CoO}_2$, and O2- $\text{Li}_{0.15}\text{CoO}_2$. Indexation of the peaks was done in the hexagonal system. * indicates the position of the (002) peak of the remaining sodium phase. † indicates an unassigned peak, probably due to the remaining sodium phase modified by electrochemical deintercalation. G = peak due to the graphite used for the batteries. ‡ = peaks due to the sample holder.

On Fig. 5, the gradual disappearance of the original (002) peak at $2\theta = 18.66^\circ$ and the appearance of a new peak at a lower angle ($2\theta = 17.95^\circ$) during further lithium extraction clearly confirm the existence of the two-phase domain ($0.72 < x \leq 0.94$), resulting from the voltage profile analysis.

T[#]2- Li_xCoO_2 ($0.52 < x \leq 0.72$).—All the Li_xCoO_2 samples with $0.52 < x \leq 0.72$ exhibit similar single-phase XRD patterns. We called this phase T[#]2 for reasons explained in the following discussion. Mendiboure *et al.* reported that the first voltage plateau in the O2- Li_xCoO_2 system was due to an O2 → O2* transformation involving only a change of the cell parameters.⁴ However, the XRD pattern exhibits two peaks that could be indexed in the hexagonal system as (111) at $2\theta = 67.5^\circ$ and (113) at $2\theta = 73.4^\circ$ (Fig. 6), which are forbidden in the $P6_3mc$ space group. This indicates that the system does not exhibit the O2 stacking anymore. XRD simulations showed that the only stacking modifications that yield the appearance of the (111) and (113) peaks while losing the 6_3 symmetry axis are the gliding of one CoO_2 layer out of two. We therefore simulated XRD patterns, using the DIFFaX program, of structures deriving from the O2 one by gliding every second CoO_2 layer in the $(1/2, 1/2, 0)$ and $(1/3, 1/6, 0)$ direction, respectively, and by different magnitudes. The corresponding results will be published elsewhere. All these structures surprisingly exhibit quite similar XRD patterns,

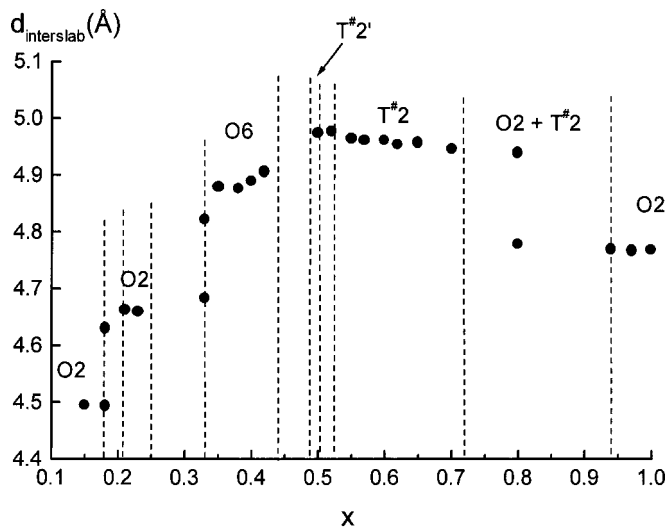


Figure 7. Evolution of the interslab distance (c parameter/number of sheets required to describe the cell) vs. lithium concentration in Li_xCoO_2 .

but the structure deriving from the O2 one by gliding every second CoO_2 layer by $(1/3, 1/6, 0)$ better reflects the experimental pattern. In their study of the O2- LiCoO_2 system, Paulsen *et al.* also noted the appearance of the (111) and (113) peaks by *in situ* XRD for $0.5 < x < 0.7$ and suggested that such a $(1/3, 1/6, 0)$ sheet gliding can be responsible for the appearance of the new diffraction lines, but they did not characterize this stacking at that time.⁵ They, however, observed similar extra peaks for the T2- $\text{Li}_{2/3}\text{Ni}_{1/3}\text{Mn}_{2/3}\text{O}_2$ phase synthesized by ion exchange from the P2- $\text{Li}_{2/3}\text{Ni}_{1/3}\text{Mn}_{2/3}\text{O}_2$ one. In this case, they characterized the new T2 stacking by neutron diffraction, and showed that this stacking cannot be described by the usual A, B, C positions of a triangular cell. The space group used was thus the orthorhombic $Cmca$ one and the lithium ions occupy distorted tetrahedral sites. In our case, the gliding of every second CoO_2 layer by $(1/3, 1/6, 0)$ from the O2 stacking yields the same oxygen stacking as that observed by Paulsen *et al.* for the T2- $\text{Li}_{2/3}\text{Ni}_{1/3}\text{Mn}_{2/3}\text{O}_2$. Figure 8 shows this gliding in projection on the (110) plane. The two oxygen layers, above and below the lithium layer situated at $z = 0.25$ are displayed. The lithium sites available are unconventional in such layered oxides. However, XRD does not allow one to determine the exact position of the lithium ions. Three tetrahedral sites are available, one 8e and two 8f ones (Fig. 8 and 9). The 8e site corresponds to a distorted LiO_4 tetrahedron with equal Li-O distances, but angles differing from those in a nondistorted tetrahedron. The two 8f sites correspond to two other distorted tetrahedra, with different angles and Li-O distances. These two 8f sites differ in their connection with the CoO_6 octahedra: one shares only edges, whereas the other shares faces.

In their neutron diffraction study of $\text{Li}_{2/3}\text{Ni}_{1/3}\text{Mn}_{2/3}\text{O}_2$, Paulsen *et al.* showed the existence of a Ni/Mn ordering in the slab and assumed that this was at the origin of the formation of the new stacking. They placed the lithium ions in the distorted tetrahedral site that corresponds to our 8e one.⁶

We called T[#]2- Li_xCoO_2 the phases obtained for O2- LiCoO_2 with $0.52 < x \leq 0.72$, as the lithium ions occupy a tetrahedral site and two layers are required to describe the unit cell. In the nomenclature of the layered oxides using the O, T, P letters followed by the number of the layers in the cell, all the atoms are in the A, B, and C positions of triangular lattice, which is not the case here. Therefore, we propose to use T[#]2 instead of T2 to avoid any confusion. Indeed, following the previous nomenclature, T2 would correspond to an ABCBA oxygen packing (identical to the O2 one) with all the lithium ions in tetrahedral sites.

Table I. Cell parameters of the Li_xCoO_2 samples.

1	2.80357(2)		9.5372(6)	O2	} Hexagonal
0.97	2.80131(7)		9.5332(3)	O2	
0.94	2.8011(1)		9.5389(7)	O2 (with some T#2)	} Hexagonal
0.72	2.8179(1)	4.8380(1)	9.89237(6)	T#2 (with some O2)	
0.65	2.8092(1)	4.8390(1)	9.91938(3)	T#2	} Orthorhombic
0.61	2.80969(3)	4.84997(7)	9.9082(2)	T#2	
0.57	2.8060(1)	4.83212(9)	9.9239(4)	T#2	} Orthorhombic
0.55	2.80733(8)	4.8291(1)	9.9262(2)	T#2	
0.52	2.8050(1)	4.8271(1)	9.9521(6)	T#2	} Orthorhombic
0.50	2.8122(1)	4.8357(3)	9.9497(2)	T#2'	
0.42	2.8108(3)		29.433(1)	O6 (with some T#2')	} Hexagonal
0.40	2.8119(2)		29.333(1)	O6	
0.37	2.8472(5)		29.3121(7)	O6	} Hexagonal
0.35	2.8070(3)		29.2700(9)	O6	
0.33	2.8116(1)		29.1879(7)	O6 (with some O2)	} Hexagonal
0.24	2.8141(1)		9.3226(7)	O2	
0.23	2.8138(1)		9.323(1)	O2	} Hexagonal
0.21	2.8141(1)		9.324(2)	O2	
0.15	2.8302(1)		8.9872(9)	O2	} Hexagonal
				O2	

A refinement of the structure of the $\text{T}^{\#2}\text{-Li}_{0.61}\text{CoO}_2$ phase was thus done in the Cmca orthorhombic space group, where the cobalt ions occupy a 4a position and oxygen an 8f position. As we cannot determine the lithium ion position by XRD, we fixed it in the 8e sites by its similarity with the $\text{T2-Li}_{2/3}\text{Ni}_{1/3}\text{Mn}_{2/3}\text{O}_2$ phase. However, adjacent 8e sites are very close, and therefore cannot be occupied simultaneously. Due to the large number of available sites [two positions for x lithium ($0.52 \leq x < 0.72$)], a lithium/vacancy ordering in the material should be considered, but this is not evidenced by XRD. In the refinement, a partial occupancy of the lithium site ($x/2$) was assumed, and we used the lithium amount determined from the voltage of the battery after the relaxation and the $V = f(x)$ curve to describe this phase (Table II). A neutron and electron diffraction study are required, to ascertain the lithium position and to check if the phase does exhibit lithium/vacancy ordering or not.

The atomic positions to be refined are the y and z coordinates of oxygen. We also refined the occupation ratio of the cobalt site, the

preferential orientation, and the cobalt and oxygen ions atomic displacement parameters. The lithium atomic displacement parameter was fixed to a value usually observed in layered oxides.¹⁴ The experimental and calculated diffractograms are represented in Fig. 10. The results of this refinement are given in Table II.

The refinement shows that the particles exhibit a weak tendency to be oriented perpendicular to the c axis (Table II) in agreement with the plate-like shape of the particles of the starting phase.³ According to the refined atomic positions for the oxygen ions, a lithium ion situated in the 8e site defined in Table II, yields two Li-O distances equal to 2.044(3) Å and two others equal to 2.070(3) Å. The huge increase of the interslab distance observed for the $\text{O2} \rightarrow \text{T}^{\#2}$ transformation (Fig. 7) allows therefore the Li-O distances to be reasonable. Note that the reliability factors obtained for the Rietveld refinement are satisfactory, but not so small, which might indicate the presence of stacking faults that we will investigate in detail in a forthcoming paper.

$\text{T}^{\#2'}\text{-Li}_{0.50}\text{CoO}_2$.—A $\text{T}^{\#2'}$ - Li_xCoO_2 phase was obtained for a 4.13 V open-circuit voltage. The XRD pattern of this phase is shown in Fig. 11. We refined the cell parameters and diffraction line profile of

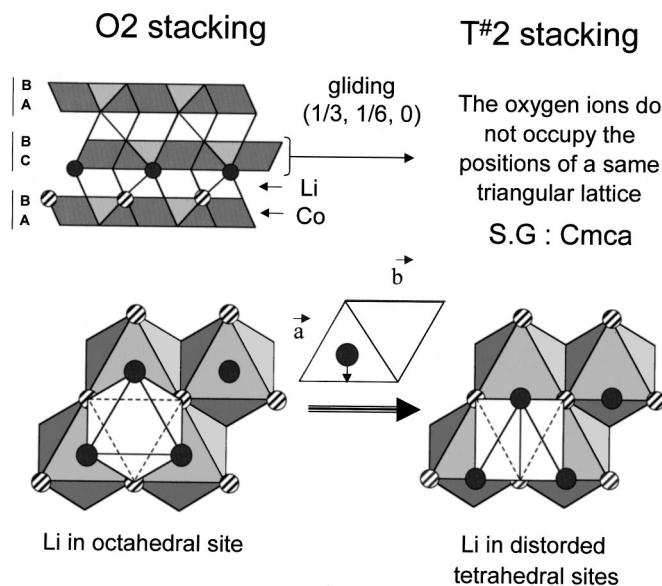


Figure 8. The sheet gliding involved in the $\text{O2} \rightarrow \text{T}^{\#2}$ transformation in the projection on the (110) plan. The two oxygen layers, above (black) and below (hatched) the lithium layer situated at $z = 0.25$, are displayed. The lithium sites in O2 and $\text{T}^{\#2}$ structures are also shown.

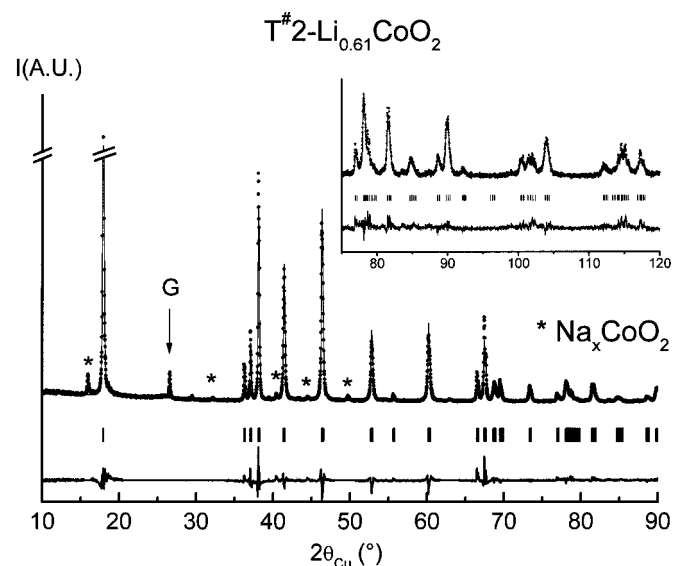


Figure 9. The $\text{T}^{\#2}$ stacking of Li_xCoO_2 phases ($0.51 < x \leq 0.72$). The distorted sites available for the lithium ions are displayed.

Table II. Rietveld refinement of the $T^{\#2}$ - $\text{Li}_{0.61}\text{CoO}_2$ XRD pattern.

$T^{\#2}$ - $\text{Li}_{0.61}\text{CoO}_2$ (electrochemical deintercalation with intermediate relaxation periods)

Space group: $Cmca$ Constraints

$a = 2.80969(3) \text{ \AA}$ Li position and concentration

$b = 4.84997(7) \text{ \AA}$ $B(\text{Li}) = 1.2 \text{ \AA}^2$

$c = 9.9082(2) \text{ \AA}$

Atom	Site	Wyckoff positions			Occupancy	B (\AA^2)
Li (1)	8e	1/4	5/12	1/4	0.31	1.2
Co (1)	4a	0	0	0	0.99(2)	0.25(7)
O (1)	8f	0	0.838(2)	0.598(2)	1.00	0.7(3)

Conditions of the run

Temperature, 300 K

Angular range, $10^\circ \leq 2\theta \leq 120^\circ$

Step scan increment (2θ), 0.02°

Zero point (2θ), $0.021(6)^\circ$

Number of fitted parameters, 18

Profile parameters

Pseudo-Voigt function

$PV = \eta L + (1 - \eta)G$ with $\eta = \eta_0 + X(2\theta)$

Halfwidth parameters

$\eta_0 = 0.64(6)$

$X = 0.004(1)$

$U = 0.05(2)$

$V = 0.03(1)$

$W = 0.006(2)$

Preferential orientation of the articles perpendicular to the c axis: 1.018(6)

Conventional Rietveld R factors for points with Bragg contribution

$R_{wp} = 15.6\%$; $R_B = 3.8\%$

Note: standard deviations have been multiplied by the Scorer number (3.16) to correct from local correlations.⁸

the $T^{\#2'}$ phase in the $Cmca$ space group (a second phase due to the sample holder in the refinement was also considered and the two 2θ regions of the most intense peaks of graphite were excluded). The resulting cell parameters for this phase are given in Table I. As the $T^{\#2'}$ phase was obtained from a mixture containing some PTFE, a strong preferential orientation is observed. As this pattern is very similar to that of the $T^{\#2}$ phase, no distinction between these two phases can be made by XRD, so that the $T^{\#2} + T^{\#2'}$ two-phase domain is not observed for $x = 0.52$ (Fig. 5). Paulsen *et al.* also reported that this phase transformation was not detected by *in situ* XRD.⁵

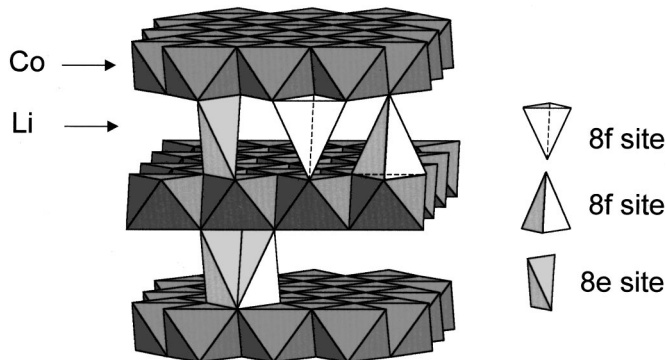


Figure 10. Observed and calculated XRD profiles for a $T^{\#2}$ phase: (●) observed; (—) calculated; lower trace: difference plot; bars: reflections.* indicates the position of the major peaks of the remaining sodium phase. G = peak due to the graphite used in the battery.

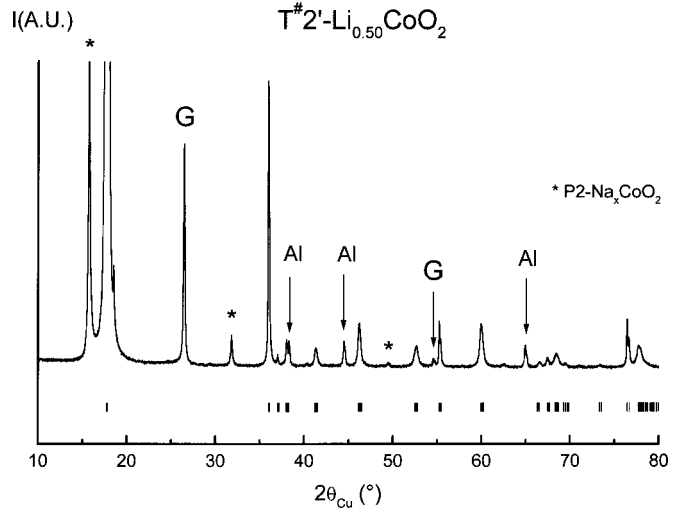


Figure 11. Observed XRD profiles for a $T^{\#2'}$ phase obtained at 4.13 V; bars: reflections in the $Cmca$ space group. * indicates the position of the major peaks of the remaining sodium phase. G = peak due to the graphite used in the battery. Al = peaks due to the sample holder.

In contrast, the two-phase domain leading to the 4.18 V plateau ($T^{\#2'} \rightarrow O6$) is seen in the $x = 0.49$ XRD pattern (Fig. 5). The peak situated at $2\theta = 18.13^\circ$ gives evidence of the O6 phase formation. The $T^{\#2'} \rightarrow O6$ phase transition is associated with a decrease in the interslab space (Fig. 7).

$O6\text{-Li}_x\text{CoO}_2$ ($0.33 < x < 0.42$).—The complete XRD pattern of the $\text{Li}_{0.37}\text{CoO}_2$ phase (Fig. 6) is characteristic of the O6 stacking (Fig. 12). This structure is observed in the $0.33 < x < 0.42$ composition range. The O6 stacking is described using the $R\bar{3}m$ space group, where the lithium ions occupy octahedral sites (6c position) and where two different cobalt layers [Co(1) in 3a and Co(2) in 3b] exist. There are also two types of oxygen ions: O(1) and O(2), both in 6c positions. In every second layer, the cobalt octahedra share only faces with the lithium ones, whereas in the other layer, the cobalt octahedra share only edges with the lithium ones. We refined the structure of one O6 phase by the Rietveld method from the XRD pattern.

The lithium position was fixed, and we used the lithium concentration determined from the voltage of the battery after the relaxation and the $V = f(x)$ curve. The atomic positions to be refined were the z coordinates of oxygen. We also refined the occupation ratio of the cobalt ions, the preferential orientation and the cobalt and oxygen atomic displacement parameters. The lithium atomic displacement parameter was fixed to a value usually observed in such compounds.¹⁴ The experimental and calculated diffractograms are shown in Fig. 13. The results are given in Table III.

The refinement shows that the particles do not exhibit any preferential orientation (Table III). In this structure, with two types of cobalt ions in different crystallographic sites, each independent oxygen position gives rise to two oxygen layers belonging to the same CoO_2 sheet, so that the space group chosen allows the differentiation of the CoO_2 layers. Considering these remarks, and the fact that this structure was found to be stable for lithium concentrations close to 0.5, Mendiboure *et al.* suggested that the trivalent cobalt cations could be mainly segregated in the sheets in which CoO_6 octahedra share faces with LiO_6 , while the tetravalent cobalt would rather be in the other sheets, so that half of the cobalt sheets are destabilized whereas the other half is stabilized with respect to the O2 structure with this composition.⁴

The refinement yields different Co-O distances, depending on the type of cobalt layer: the octahedra sharing faces with LiO_6 exhibit a

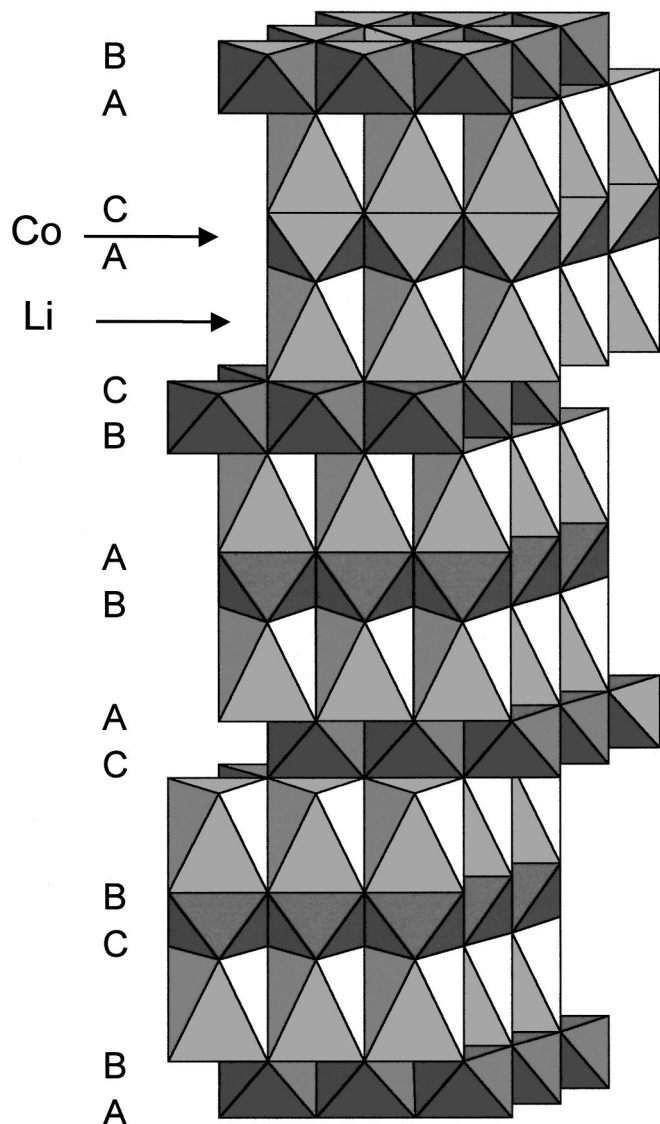


Figure 12. The O6 stacking of Li_xCoO_2 phase ($0.33 < x < 0.42$).

1.8710(1) Å Co-O distance, whereas the octahedra sharing edges with LiO_6 exhibit a 1.8617(1) Å Co-O distance. The difference found is small, but so is the difference between the ionic radii of Co^{3+} (0.545 Å) and Co^{4+} (0.530 Å).¹⁵ These results would suggest that one CoO_2 slab out of two contains the Co^{4+} ions, corresponding to the shorter Co-O distances. This could be a way to minimize the electrostatic repulsion between Co^{4+} and lithium. However, the O6 stacking is not obtained for $x = 0.50$, as was previously observed by Mendiboure *et al.*, so that we also expect some Co^{4+} ions to be present in the cobalt layer that shares faces with LiO_6 .

One can note that the peak profile is not fully satisfactorily simulated with the Fullprof program as the XRD pattern displayed on Fig. 13 does not exhibit peak widths that strictly vary smoothly as a function of the scattering angle which yields significant reliability factors. The (110) peak situated at $2\theta = 66.6^\circ$ for instance is rather sharp as compared to the others. Furthermore, the peak width also depends on the way used to prepare the phases (with or without the use of additives). As already mentioned for the T#2 phase, this behavior could be due to the presence of some stacking faults in the material.

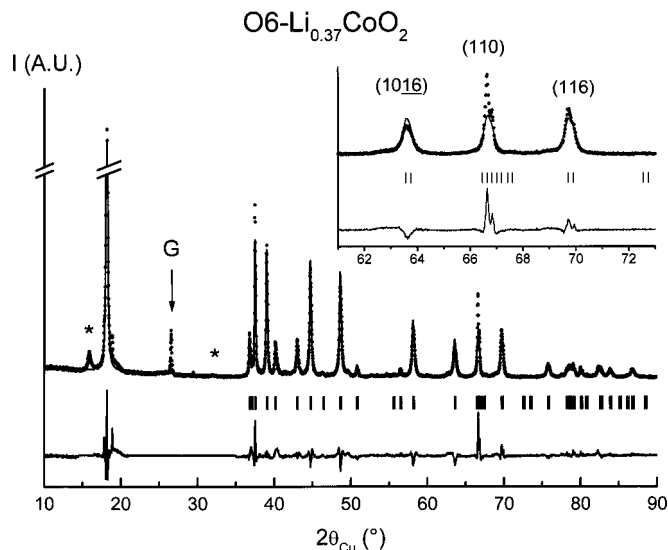


Figure 13. Observed and calculated XRD profiles for the O6- $\text{Li}_{0.37}\text{CoO}_2$ phase: (●) observed; (—) calculated; lower trace: difference plot; bars: reflections. * indicates the position of the major peaks of the remaining sodium phase. G = peak due to the graphite used in the battery.

For lower lithium amounts, the system undergoes another phase transformation that leads again to the O2 stacking with a smaller interslab space as seen in Fig. 5 by the appearance of a new peak at higher angle ($2\theta = 19^\circ$). Paulsen *et al.* also observed this transformation by *in situ* XRD.⁵

Table III. Rietveld refinement of the O6- $\text{Li}_{0.37}\text{CoO}_2$ XRD.

O6- $\text{Li}_{0.37}\text{CoO}_2$ (electrochemical deintercalation)					
Space group: $R\bar{3}m$			Constraints:		
$a_{\text{hex.}}$	$= 2.80472(5)$ Å	Li position and concentration			
$c_{\text{hex.}}$	$= 29.3121(7)$ Å	$B(\text{Li}) = 1.2$ Å ² ;			
		$B[\text{Co}(1)] = B[\text{Co}(2)]$;			
		$B[\text{O}(1)] = B[\text{O}(2)]$			
		Wyckoff positions			
Atom	Site			Occupancy	B (Å ²)
Li (1)	6c	0	0	1/12	0.37
Co (1)	3a	0	0	0	1.01(4)
Co (2)	3b	0	0	0.5	1.03(4)
O (1)	6c	0	0	0.1980(8)	1.000
O (2)	6c	0	0	0.3651(8)	1.000
Conditions of the run:					
Temperature, 300 K					
Angular range, $5^\circ \leq 2\theta \leq 120^\circ$					
Step scan increment (2θ), 0.02°					
Zero point (2θ), $-0.016(9)^\circ$					
Number of fitted parameters, 18					
Profile parameters					
Pseudo-Voigt function					
$PV = \eta L + (1 - \eta)G$ with $\eta = \eta_0 + X(2\theta)$					
Halfwidth parameters					
$\eta_0 = 1.14(6)$					
$X = -0.007(3)$					
$U = 0.4(1)$					
$V = -0.13(5)$					
$W = 0.020(6)$					
Preferential orientation of the particles perpendicular to the c axis: 1.00(2)					
Conventional Rietveld R factors for points with Bragg contribution:					
$R_{\text{wp}} = 20.2\%$; $R_{\text{B}} = 6.0\%$					
Note: standard deviations have been multiplied by the Scorer number (4.15) to correct from local correlations. ⁸					

O2-Li_xCoO₂ (0.21 ≤ x ≤ 0.24).—The XRD study of the Li_xCoO₂ phases shows that the O2 stacking is also observed for 0.21 ≤ x ≤ 0.24. Figure 6 shows the complete XRD pattern obtained for x = 0.23. The highly deintercalated phase was obtained from a mixture containing some PTFE, therefore strong preferential orientation is observed. One can also notice that the remaining sodium P2 phase has evolved, as its peak situated at low 2θ value is shifted and broadened. The cell parameters found for O2-Li_{0.23}CoO₂, reported in Table I, are in good agreement with the *in situ* XRD study of Paulsen *et al.*⁵ The emerging peak situated at 2θ = 19.66° for x = 0.20 in Fig. 5 gives evidence of a two-phase domain leading to the 4.57 V plateau.

O2-Li_xCoO₂ (x ≤ 0.15).—As our cycling curve ends at 4.6 V, we do not observe the single-phase domain corresponding to this phase in Fig. 3 and 4. However, we prepared a highly deintercalated single phase (x = 0.15), with an open-circuit voltage equal to 4.60 V. To our knowledge, this highly deintercalated O2 phase was not evidenced before.

The O2-Li_{0.15}CoO₂ phase exhibits an O2 stacking (Fig. 5 and 6) with a small interslab distance [4.497(3) Å Table I and Fig. 7]. Such a drop of the interslab spacing was also observed for highly deintercalated phases such as Li_xCoO₂¹⁶ and Li_xNiO₂,¹⁷⁻²⁰ but in these cases the slope was even larger as the lithium concentration reached was lower than 0.15. One can note in Fig. 6 that the diffraction peaks of this phase are broad, showing that it is not well crystalline.

Electronic properties.—Electronic conductivity.—Figure 14 shows the variation vs. reciprocal temperature of the electronic conductivity recorded for the Li_xCoO₂ samples, with x ranging from 1 to 0.38. The activation energy does not strictly obey an Arrhenius law, as it varies slightly with temperature. When lithium is deintercalated, the electronic conductivity increases and the activation energy decreases rapidly. Indeed, lithium deintercalation entails an oxidation of the cobalt ions to their tetravalent state. The conductive electrons are thus situated in the Co t₂ band, which can overlap through the common edge of the CoO₆ octahedra and can lead to a delocalization. However, although the conductivity values are quite high, the electronic conductivity remains thermally activated for all compositions.

However, the pellets used for the electronic measurements were not sintered before lithium deintercalation, because of the metastability of the O2-LiCoO₂ starting phase. A sintering process is usually required for these measurements to improve the intergrain contacts in the material, so that in our case an alteration of the conductivity value is expected. As measurements reported in Ref. 21 for the O3-Li_xCoO₂ phases were carried out with pellets sintered at 800°C for 12 h before the lithium deintercalation, it is interesting to show to what extent the absence of sintering can affect electric conductivity measurements. Figure 15 shows the variation vs. reciprocal temperature of the electronic conductivity of two O3-Li_{0.60}CoO₂ materials, one having been sintered before the electrochemical deintercalation and the other not. For comparison, the variation of the electronic conductivity of T[#]2-Li_{0.61}CoO₂ has been plotted. The shape of the curve and the conductivity values obtained for the sintered pellet of the O3-Li_{0.60}CoO₂ phase are in good agreement with those reported in Ref. 21. The decrease of the electronic conductivity when the temperature increases indicates a metallic character, revealing that an electronic delocalization occurs in this material. However, the thermal variation obtained for the same composition, but for the unsintered pellet is completely different. The electronic conductivity is thermally activated, characterizing an activated phenomenon.

As shown in Fig. 15, the evolution of conductivity vs. the reciprocal temperature for the T[#]2-Li_{0.61}CoO₂ material is quite similar to the one obtained for the O3-Li_{0.60}CoO₂ unsintered pellet. We may thus expect the T[#]2-Li_{0.61}CoO₂ material to have exhibited a metallic behavior if the pellet could have been sintered before the deinterca-

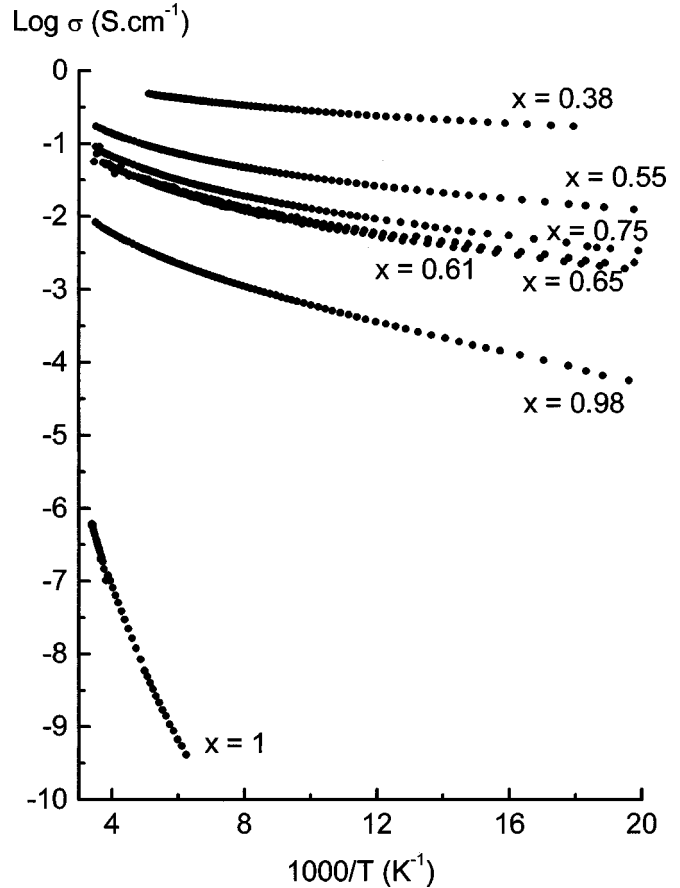


Figure 14. Variation of the logarithm of the electrical conductivity vs. reciprocal temperature of the Li_xCoO₂ phase (0.38 ≤ x ≤ 1).

lation. This clearly shows that the electronic conductivity measurements on unsintered pellets must be considered with caution.

Thermoelectric power.—Thermoelectric power measurements of various Li_xCoO₂ compositions are shown in Fig. 16. These measurements are not sensitive to the pellet sintering issue, so they could provide information on the electronic properties of the bulk.

The positive values of the Seebeck coefficient obtained for x > 0.55 establish that electron holes are the prevailing charge carriers, in good agreement with the formation of holes in the t₂ Co band. The high values of the thermoelectric power obtained for x = 0.98 and x = 0.97 are typical of a small polaronic behavior, in good agreement with the results obtained by electronic conductivity measurements. The lower Seebeck coefficient values obtained for x = 0.97 result from an increase in the number of charge carriers as oxidation of the diamagnetic Co³⁺ ions to paramagnetic Co⁴⁺ ions proceeds. Nevertheless, for both materials, the temperature dependence reflects a complex behavior.

For the most deintercalated phases (0.55 < x < 0.75), the quasi linearity of the plots and the low values of the Seebeck coefficient, which tends to zero when the temperature decreases, are typical of a metallic behavior. For x = 0.75, which corresponds to the O2-T[#]2 two-phase domain, an intermediate behavior is observed. For the O6 phase (x = 0.38), the Seebeck coefficient is quasi temperature-independent and is very close to zero. This behavior clearly indicates that an electronic delocalization occurs in this phase.

The α = f(T) plots of the O2-Li_xCoO₂ phases are very similar to those reported for the O3-Li_xCoO₂ phases (1 ≤ x ≤ 0.60). For the O3 system, these measurements coupled with the electronic con-

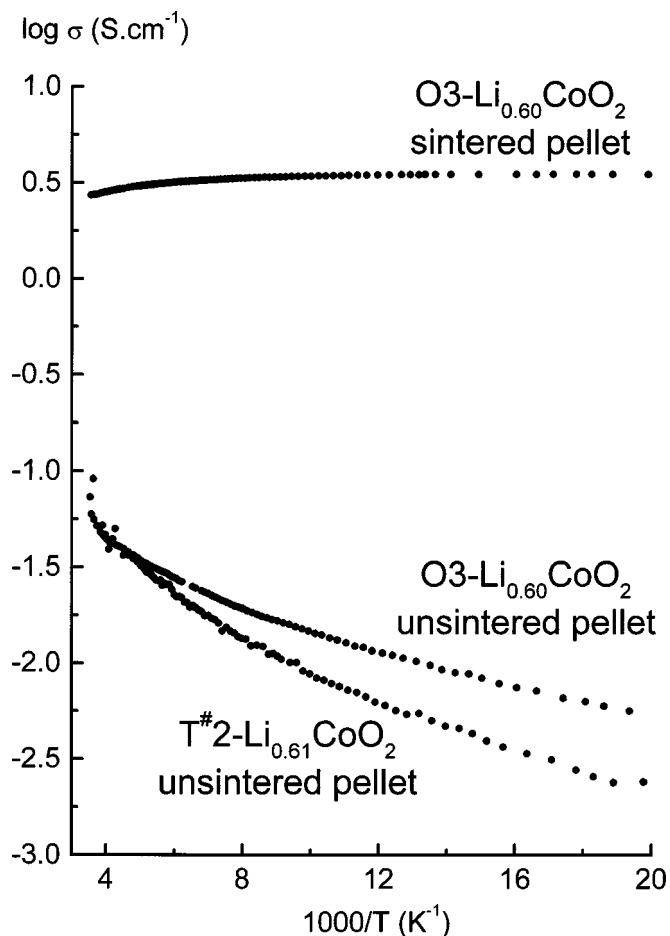


Figure 15. Variation of the logarithm of the electrical conductivity vs. reciprocal temperature of the O3-Li_{0.60}CoO₂ phases measured on sintered and unsintered pellets and of the O2-Li_{0.61}CoO₂ phase measured on an unsintered pellet.

ductivity and the ⁷Li NMR ones were indicative of a nonmetal to metal transition.²¹

Discussion on the electronic properties.—In O2-LiCoO₂, as shown by our earlier magnetic study, the Co³⁺ ions are in a low spin configuration, so that they are diamagnetic ($t_2^6e^0$) and should not give rise to conduction.³ Lithium deintercalation, which increases the number of tetravalent cobalt ions, tends to decrease the activation energy and to increase the conductivity. Indeed, the conductive electrons are situated in the Co t_2 orbitals, which can overlap through the common edge of the octahedra and can lead to a delocalization. As discussed by Goodenough, in transition metal oxides, the electronic delocalization through overlapping t_2 orbitals (edge sharing octahedra) is expected if the bands are not completely filled and if the metal-metal distance is smaller than an empirical value R_c .²² For O2-Li_xCoO₂, R_c varies from 2.900 Å for $x = 1$ to 2.850 Å for $x = 0.38$. In the case of O3-Li_xCoO₂, the t_2 orbital overlap leads to a metallic phase for $x \leq 0.74$, in agreement with Goodenough's criterion.²¹ In the case of the O2-Li_xCoO₂ phases, the metal-metal distance ($d_{\text{Co-Co}}$) is always smaller than the critical R_c value ($d_{\text{Co-Co}}$ always between 2.787 and 2.847 Å; see a_{hex} , a_{orth} , and b_{orth} $\sqrt{3}$ in Table I), so that an electronic delocalization is expected as soon as a high enough amount of lithium ions are removed. The thermoelectric power measurements clearly show this localized to itinerant electrons evolution. The O2 \rightarrow T[#]2 transformation appears therefore to be correlated with a nonmetal to metal transition. The

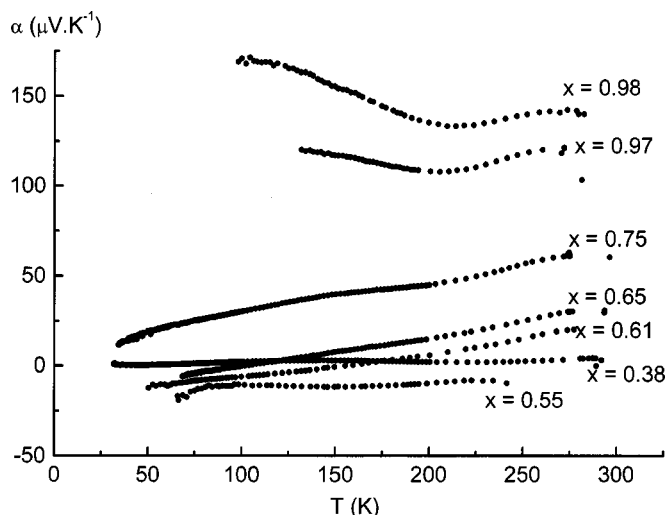


Figure 16. Thermal variation of the Seebeck coefficient of the Li_xCoO₂ phases ($0.38 \leq x \leq 0.98$).

metallic character of the O6 phase can appear contradictory with charge ordering between the cobalt ions, but as already mentioned this stacking is stable for $0.33 < x < 0.42$, so that some Co⁴⁺ ions must be present in the Co³⁺ slab. An electronic delocalization can thus occur in both types of CoO₂ slabs.

NMR measurements.—Since XRD yields long-range structural information, we used ⁷Li NMR to obtain information on the local structure around lithium. Indeed, NMR spectroscopy is very sensitive to the presence of a spin density at the site of the nucleus.

Figure 17 shows the ⁷Li MAS NMR spectra of the starting O2-LiCoO₂ and of some deintercalated compounds. As we reported elsewhere, O2-LiCoO₂ exhibits a single narrow signal situated at 0 ppm, indicating that no paramagnetic cobalt ions related to oxygen deficiency is present in the starting phase.³ Indeed, Co³⁺ is diamagnetic so that no hyperfine interaction is expected, as also observed for stoichiometric O3-LiCoO₂.^{21,23-29} On the opposite the presence of single electrons due to some paramagnetic cobalt ions related to nonstoichiometry yields additional shifted signals.²⁹

The spectra recorded for $0.97 \leq x \leq 1$ (Fig. 18) all exhibit the same single signal, and therefore are not shown in Fig. 17. However, the magnitude of the signal changes with x , as shown in Fig. 18. The spectra are shown in a common absolute scale of magnitude, taking into account the amount of material and the number of scans used. All the other NMR parameters including the spinning frequency are kept constant. In Fig. 18 we give the integrated intensity of each signal including the spinning side bands. Of course, the quantification is not strict, as the magnitude of the signal also depends on the sequence used to record it. In another study, we reported that a synchronized echo pulse sequence was not suited to record ⁷Li NMR spectra of deintercalated phases; indeed, the lithium ions motion in the interslab space modifies the spin system between the two required pulses, leading to the nonrefocusing of part of the signals.³⁰ However, it is also well known that a single pulse sequence underestimates broad signals. We therefore show the evolution of the signals recorded with both types of sequence, giving the relative intensity of the observed peak. The values obtained clearly show a stronger decrease in the signal intensity than expected by considering the small decrease in lithium concentration. Similar results were obtained for the O3-Li_xCoO₂ phases with $0.94 < x \leq 1.0$.²¹ The gradual loss of observability for the ⁷Li NMR signal observed in both systems is considered to be due to the presence of localized Co⁴⁺ in the material. Indeed, for this lithium amount, some cobalt ions are oxidized to the Co⁴⁺ state, with the t_2^5 elec-

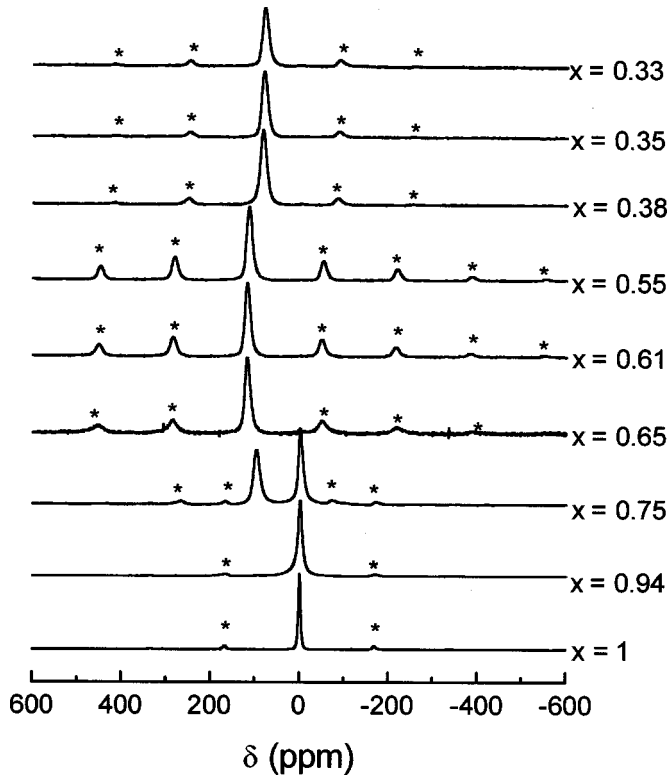


Figure 17. ${}^7\text{Li}$ MAS NMR spectra of various Li_xCoO_2 ($0.33 \leq x \leq 1$) deintercalated phases recorded with a single-pulse sequence and a 13 kHz spinning speed. * indicates the spinning side bands.

tronic configuration. As the single electron is situated in a t_2 orbital of the Co^{4+} ions, the transfer of hyperfine interaction toward lithium can occur directly through the common edge of the CoO_6 and LiO_6 octahedra. The transferred hyperfine interaction, as well as the dipolar contribution, is then so strong that the ${}^7\text{Li}$ NMR signal is no longer observable. Electronic hopping between cobalt ions also occurs, and since the NMR time scale ($\sim 10^{-6}$ s) is considerably larger than the electronic hopping one ($\sim 10^{-12}$ s), the single electron may interact with many Li^+ ions during the recording of the free induction decay. This leads to a loss of observability higher than that calculated considering that each Co^{4+} ion interacts with six Li^+ ions (*i.e.*, for $x = 0.97$, one would expect a minimum of 82% observability in the absence of electronic hopping).

Figure 17 shows the NMR signal recorded for further deintercalated Li_xCoO_2 phases. We observed the emergence of a new signal, shifted by 100 ppm, characterizing the $T^{\#2}$ phase. For $x = 0.75$, the presence of the two signals confirms the biphasic character of this material. For $x < 0.75$, the 0 ppm signal has disappeared, and the new signal shifts further (≈ 120 ppm). The type of interaction experienced by lithium has changed, as it leads now to the observation of a shifted signal. These results are in good agreement with the thermoelectric power measurements, which suggest that the $\text{O2} \rightarrow T^{\#2}$ phase transformation is correlated with a nonmetal to metal transition. The NMR signal observed for the $T^{\#2}$ phases is therefore a Knight shift (due to the participation of the 2s orbital of Li to the density of state at the Fermi level), characteristic of a metallic phase. The same behavior was observed for the $\text{O3-Li}_x\text{CoO}_2$ system for $x \leq 0.74$.²¹

One can notice in Fig. 17 that the expansion of the spinning side bands is larger for $T^{\#2}$ phases than for O2 ones. Simulations of the signal shape showed that this broadening is due to a quadrupolar interaction resulting from an asymmetric electrical field gradient around the lithium ions, which confirms that they are situated in

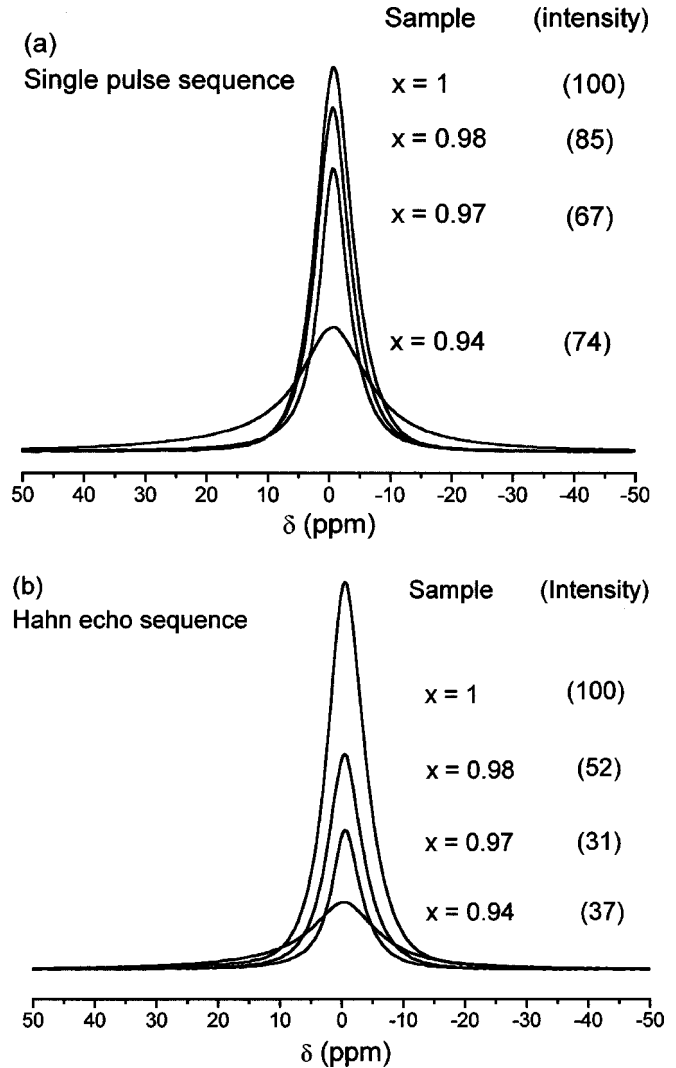


Figure 18. ${}^7\text{Li}$ MAS NMR spectra of Li_xCoO_2 ($0.94 \leq x \leq 1$) deintercalated phases recorded with a 10 kHz spinning speed and (a) a single-pulse sequence and (b) a Hahn echo sequence. Spectra are plotted in an absolute intensity scale. The total integrated intensity of the signals is also given.

sites which exhibit a lower symmetry than the starting octahedral one. However, NMR experiments using only one field do not allow one to determine which tetrahedral site (8e or 8f) is occupied by the lithium ions.

For lithium concentrations lower than 0.50, the Knight-shifted signal is less shifted (≈ 100 ppm), and the extent and intensity of the spinning side bands decreases again. Indeed, for $0.33 \leq x \leq 0.39$, the Li_xCoO_2 phases adopt the O6 stacking, in which the lithium ions occupy more symmetric sites. The observed decrease in the shift for decreasing values of x seems counterintuitive, since more charge carriers should be present upon further oxidation of Co^{3+} to Co^{4+} . However, one has also to take into account the detailed structural parameters of the materials, which are very important for the density of states at the Fermi level, and therefore for the Knight-shift observed.

Conclusions

Lithium deintercalation from O2-LiCoO_2 is complex as it involves several structural rearrangements. All these transformations are reversible for $0.16 \leq x \leq 1$ and imply CoO_2 slab glidings, nonmetal to metal transition, and possible lithium/vacancy ordering. We showed that the electrostatic repulsion between cobalt and lithium

ions through the common face of their octahedra is strong enough to shift the lithium and cobalt ions from their ideal position in the O2 starting phase.³ Lithium deintercalation involves cobalt oxidation to the tetravalent state, which should imply even stronger electrostatic repulsion between cobalt and lithium in the O2 structure. We believe that the structural transformations observed as lithium is deintercalated from the O2 structure are a way to minimize this strong repulsion. For $0.94 < x < 1$, the O2 structure remains stable as lithium vacancies can be formed in the sites sharing a face with the Co^{4+} octahedra, so that strong Co^{4+} -Li repulsion can be avoided. We showed by thermoelectric power and ^7Li MAS NMR measurements that as soon as $x < 0.94$, a nonmetal to metal transition occurs in the material. Because of the electronic delocalization on the cobalt ions, if the structure remained O2, all the lithium ions would undergo the same strong electrostatic interactions. The structural evolution to the $\text{T}^{\#2}$ stacking thus allows lithium ions to be placed in tetrahedral sites which do not share faces with CoO_6 octahedra so that the Co-Li repulsions are minimized.

For $x < 0.50$, the O6 stacking is stabilized. Because this structure contains two types of CoO_2 layers, a segregation of the Co^{4+} ions into the layers that do not share faces with the octahedral lithium site, could minimize the electrostatic repulsion. A high enough number of Co^{4+} ions would therefore be necessary for this stacking to form, and it occurs for $x < 0.5$.

The transformation of O6 back to O2 after further deintercalation is connected with a decrease in the interslab distance, which becomes smaller than that of the starting O2 phase. This indicates an increase in the covalency within the CoO_2 layers. The formal charge on the cobalt ions decreases, and so does the repulsion between Co^{n+} - Li^+ ions though the common face of their octahedra. The O2 stacking is thus again stable. The $\text{O6} \rightarrow \text{O2}$ phase transformation could be induced because the number of tetravalent cobalt ions becomes too high in the Co^{3+} (face sharing octahedra) layer.

The only phase transformation that does not seem to be induced by the minimization of electrostatic repulsions between Co^{4+} and Li^+ ions is the $\text{T}^{\#2} \rightarrow \text{T}^{\#2'}$ one, which appears for $x = 0.50$ and is thought to correspond to a lithium/vacancy ordering as was assumed in the $\text{O3-Li}_x\text{CoO}_2$ system. However, no sign of lattice distortion that could be due to this ordering was recorded by XRD.

Acknowledgments

The authors thank L. Croguennec for fruitful discussions, C. Denage for technical assistance, and Région Aquitaine for financial support.

Université de Bordeaux I assisted in meeting the publication costs of this article.

References

1. C. Delmas, J. J. Braconnier, and P. Hagenmuller, *Mater. Res. Bull.*, **17**, 117 (1982).
2. C. Delmas, C. Fouassier, and P. Hagenmuller, *Physica B*, **99**, 81 (1980).
3. D. Carlier, I. Saadoune, L. Croguennec, M. Ménétrier, E. Suard, and C. Delmas, *Solid State Ionics*, **144**, 263 (2001).
4. A. Mendiboure, C. Delmas, and P. Hagenmuller, *Mater. Res. Bull.*, **19**, 1383 (1984).
5. J. M. Paulsen, J. R. Mueller-Neuhaus, and J. R. Dahn, *J. Electrochem. Soc.*, **147**, 508 (2000).
6. J. M. Paulsen, R. A. Donaberger, and J. R. Dahn, *Chem. Mater.*, **12**, 2257 (2000).
7. J. M. Paulsen, D. Larcher, and J. R. Dahn, *J. Electrochem. Soc.*, **147**, 2862 (2000).
8. J. Rodriguez-Carvajal, Laboratoire Leon Brillouin (CEA-CNRS), <http://www-llb.cea.fr/fullweb/powder.htm>
9. C. P. Slichter, *Principles of Magnetic Resonance*, Springer-Verlag, Berlin (1992).
10. P. Dordor, E. Marquestaut, and G. Villeneuve, *Rev. Phys. Appl.*, **15**, 1607 (1980).
11. J. N. Reimers and J. R. Dahn, *J. Electrochem. Soc.*, **139**, 2091 (1992).
12. J. M. Paulsen, C. L. Thomas, and J. R. Dahn, *J. Electrochem. Soc.*, **146**, 3560 (1999).
13. J. M. Paulsen, C. L. Thomas, and J. R. Dahn, *J. Electrochem. Soc.*, **147**, 861 (2000).
14. A. Rougier, P. Gravereau, and C. Delmas, *J. Electrochem. Soc.*, **143**, 1168 (1996).
15. R. D. Shannon and C. T. Prewitt, *Acta Crystallogr., Sect. B: Struct. Crystallogr. Cryst. Chem.*, **25**, 925 (1969).
16. G. G. Amatucci, J. M. Tarascon, and L. C. Klein, *J. Electrochem. Soc.*, **143**, 1114 (1996).
17. T. Ohzuku, A. Ueda, and M. Nagayama, *J. Electrochem. Soc.*, **140**, 1862 (1993).
18. W. Li, J. N. Reimers, and J. R. Dahn, *Solid State Ionics*, **67**, 123 (1993).
19. L. Seguin, G. Amatucci, M. Anne, Y. Chabre, P. Strobel, J. M. Tarascon, and G. Vaughan, *J. Power Sources*, **81-82**, 604 (1999).
20. A. N. Mansour, X. Q. Yang, X. Sun, J. Mc Breen, L. Croguennec, and C. Delmas, *J. Electrochem. Soc.*, **147**, 2104 (2000).
21. M. Ménétrier, I. Saadoune, S. Levasseur, and C. Delmas, *J. Mater. Chem.*, **9**, 1135 (1999).
22. J. B. Goodenough, *Prog. Solid State Chem.*, **5**, 278 (1971).
23. B. Ouyang, X. Cao, H. W. Lin, S. Slane, S. Kostov, M. d. Boer, and S. G. Greenbaum, *Mater. Res. Soc. Symp. Proc.*, **369**, 59 (1995).
24. M. Carewska, S. Scaccia, S. Arumugam, Y. Wang, and S. Greenbaum, *Solid State Ionics*, **93**, 227 (1997).
25. T. J. Boyle, D. Ingersoll, T. M. Alam, C. J. Tafoya, M. A. Rodriguez, K. Vanheusden, and D. H. Dougherty, *Chem. Mater.*, **10**, 2270 (1998).
26. R. Alcantara, P. Lavela, J. L. Tirado, E. Zhecheva, and R. Stoyanova, *J. Electroanal. Chem.*, **454**, 173 (1998).
27. M. P. J. Peeters, M. J. Van Bommel, P. M. C. Neilen-ten Wolde, H. A. M. Van Hal, W. C. Keur, and A. P. M. Kentgens, *Solid State Ionics*, **112**, 41 (1998).
28. N. Imanishi, M. Fujiyoshi, Y. Takeda, O. Yamamoto, and M. Tabuchi, *Solid State Ionics*, **118**, 121 (1999).
29. S. Levasseur, M. Ménétrier, E. Suard, and C. Delmas, *Solid State Ionics*, **128**, 11 (2000).
30. D. Carlier, M. Ménétrier, and C. Delmas, *J. Mater. Chem.*, **11**, 594 (2001).